PHYSICAL REVIEW D **82,** 094004 (2010)

Role of two-flavor color superconductor pairing in a three-flavor Nambu–Jona-Lasinio model with axial anomaly

H. Basler and M. Buballa

Institut für Kernphysik, Technische Universität Darmstadt, 64289 Darmstadt, Germany

(Received 9 August 2010; published 10 November 2010)

The phase diagram of strongly interacting matter is studied within a three-flavor Nambu–Jona-Lasinio model, which contains the coupling between chiral and diquark condensates through the axial anomaly. Our results show that it is essential to include the two-flavor color superconducting (2SC) phase in the analysis. While this is expected for realistic strange-quark masses, we find that even for equal up, down, and strange bare quark masses 2SC pairing can be favored due to spontaneous flavor symmetry breaking by the axial anomaly. This can lead to a rich phase structure, including BCS- and Bose-Einstein condensate-like 2SC and color-flavor locked phases and new endpoints. On the other hand, the low-temperature critical endpoint, which was found earlier in the same model without 2SC pairing, is almost removed from the phase diagram and cannot be reached from the low-density chirally broken phase without crossing a preceding first-order phase boundary. For physical quark masses no additional critical endpoint is found.

DOI: 10.1103/PhysRevD.82.094004 PACS numbers: 12.38.Aw, 03.75.Nt, 11.30.Rd, 12.39.−x

I. INTRODUCTION

The phase diagram of strongly interacting matter is studied with great effort, both experimentally and theoretically. From direct observations, we know that at low temperature and low chemical potential chiral symmetry is spontaneously broken and hadrons are the relevant degrees of freedom. There are strong indications from heavy-ion experiments that this is changed at high temperatures, where quarks and gluons become the relevant degrees of freedom and a so-called quark-gluon plasma (QGP) is formed (see Ref. [1] for an overview). This is also confirmed by lattice simulations of quantum chromodynamics (QCD) at nonvanishing temperature [2,3]. These calculations indicate that, for physical quark masses and vanishing chemical potential, the hadronic phase and the QGP are connected by a smooth crossover [4].

At high densities and low temperatures, on the other hand, strongly interacting matter is expected to be a color superconductor, where the quarks form Cooper pairs (for reviews, see [5–11]). This can rigorously be shown for asymptotically high densities by applying weak-coupling techniques to QCD [12–15]. Unfortunately, these methods fail at more ''moderate'' densities, which are of phenomenological interest. Moreover, because of the ''sign problem'', the regime of low temperature and nonvanishing chemical potential cannot be studied within lattice QCD. However, in model calculations one typically finds that the hadronic phase is bordered by a first-order phase boundary in the low-temperature region [16,17]. The combination of this result with the notion of the crossover at zero chemical potential then leads to the standard picture of the phase diagram, where the first-order phase transition ends at a critical end point (CEP). The latter has attracted considerable attention, as it is potentially detectable in heavy-ion experiments [18].

It is possible, however, that the phase boundary of the hadronic phase contains more than one CEP. For instance, it was found within a Nambu–Jona-Lasinio (NJL) model that imposing charge neutrality or the inclusion of vector interactions weaken the first-order phase transition and can lead to a second end point at low temperatures near the chemical-potential axis [19–21]. Beside these mechanisms, it has been shown in a Ginzburg-Landau (GL) analysis [22–24] that the interaction between the chiral and diquark condensates, induced by the axial anomaly, can also lead to such a low-temperature endpoint. This result is rather general, but it strongly depends on the values of the GL coefficients, which could not be determined within this framework. It is therefore very interesting that it has recently been confirmed explicitly within an NJL-model study [25]. Thereby the authors have included a $U_A(1)$-symmetry breaking interaction term, which connects chiral and diquark condensates. This term plays a crucial role in the GL analysis but is usually neglected in the NJL model. In Ref. [25], it was found that it indeed leads to the emergence of a second CEP if the coupling is sufficiently strong.

However, the calculations have been performed under the simplifying assumption of three quark flavors with equal masses. In this case, it appears natural that color superconducting quark matter is realized in the color-flavor locked (CFL) phase [26], where up, down, and strange quarks are paired in a very symmetric way. The authors of Ref. [25] have therefore considered only one common diquark condensate and one common chiral condensate in their analysis. The same is true for the GL analysis of Refs. [22–24] in the case of equal quark masses. Of course, the assumption of equal quark masses is quite unrealistic, leading to the question whether the second CEP can still be found in a scenario where the strange-quark mass is significantly larger than the masses of the up and down

quarks. In order to investigate this question, some generalizations of the model are necessary: When the quark masses are different, the chiral condensates will take different values for different flavors, and also the diquark condensates will depend on the flavor content of the paired quarks. In particular, at large differences between strange and nonstrange quark masses, the CFL pairing will become unfavored [27–29], and a two-flavor color superconductor (2SC) [30,31] will emerge, where only up and down quarks are paired.

In the following, we will analyze the effect of these generalizations on the phase structure. Thereby, it was our original motivation to investigate the effect of realistic mass differences. However, to our surprise, we find that even for equal bare quark masses the 2SC phase can be favored due to the coupling of the chiral and diquark condensates by the axial anomaly. As a result, we find the scenario of Ref. [25] never to be favored, not even for equal quark masses.

In the following, this will be discussed in detail. In Sec. II, we briefly introduce the model and the parameters before presenting the numerical results in Sec. III and concluding in Sec. IV.

II. THE MODEL

A. The Lagrangian

We adopt the NJL-type Lagrangian of Ref. [25],

$$\mathcal{L} = \bar{q}(i\partial\!\!\!/ - \hat{m} + \gamma_0\mu)q + \mathcal{L}_\chi^{(4)} + \mathcal{L}_d^{(4)} + \mathcal{L}_\chi^{(6)} + \mathcal{L}_{\chi d}^{(6)}, \quad (1)$$

which is based on a frequently used Lagrangian (e.g., [32–35]) extended by the interaction term $\mathcal{L}_{\chi d}^{(6)}$. It describes the dynamics of a quark field q with three color (r, g, b) and three flavor (u, d, s) degrees of freedom. The current quark masses enter through the diagonal mass matrix $\hat{m} = \mathrm{diag}_f(m_u, m_d, m_s)$ and μ is the quark chemical potential. In the present analysis, we do not impose electric or color charge neutrality constraints. These constraints play an important role in compact stars and can lead to a rather complicated phase structure [32–36]. On the other hand, they are less important in heavy-ion collisions, where the matter does not need to be locally neutral. As a first step, we therefore use a common chemical potential for all quarks in order to keep the analysis simple.

The Lagrangian Eq. (1) includes a four-point interaction in the quark-antiquark channel

$$\mathcal{L}_\chi^{(4)} = G\sum_{a=0}^{8}[(\bar{q}\tau_a q)^2 + (\bar{q}i\gamma_5\tau_a q)^2], \quad (2)$$

and a four-point interaction in the quark-quark channel

$$\mathcal{L}_d^{(4)} = H\sum_{i,j=1}^{3}[(\bar{q}i\gamma_5 t_i l_j C\bar{q}^T)(q^T Ci\gamma_5 t_i l_j q) + (\bar{q}t_i l_j C\bar{q}^T)(q^T Ct_i l_j q)]. \quad (3)$$

Here G and H are dimensionful coupling constants, $C = i\gamma^2\gamma^0$ is the charge conjugation matrix, and τ_a are the Gell-Mann matrices in flavor space, extended by $\tau_0 = \sqrt{2/3}\mathbb{1}_f$. The flavor and color structure of the quark-quark interaction is generated by the antisymmetric matrices

$$\begin{aligned} t_1 &\equiv \tau_7, & t_2 &\equiv -\tau_5, & t_3 &\equiv \tau_2, \\ l_1 &\equiv \lambda_7, & l_2 &\equiv -\lambda_5, & l_3 &\equiv \lambda_2, \end{aligned} \quad (4)$$

where λ_a are the Gell-Mann matrices in color space.

The four-point interaction terms $\mathcal{L}_\chi^{(4)}$ and $\mathcal{L}_d^{(4)}$ are symmetric under $U(3)_R \times U(3)_L$ transformations in flavor space. In order to break the $U(1)$ axial symmetry, we include the standard six-point interaction term [37,38]

$$\mathcal{L}_\chi^{(6)} = -K\{\det{}_f[\bar{q}(1+\gamma_5)q] + \det{}_f[\bar{q}(1-\gamma_5)q]\}, \quad (5)$$

which can be related to instanton effects. This term connects three incoming right-handed fields with three outgoing left-handed fields and vice versa. In principle, it can therefore couple to three quark-antiquark channels (e.g., $(\bar{u}u)(\bar{d}d)(\bar{s}s)$) as well as to one quark-antiquark channel together with one diquark and one antidiquark (e.g., $(ud)\times(\bar{u}\,\bar{d})(\bar{s}s)$). However, in Hartree approximation, which will be employed below, $\mathcal{L}_\chi^{(6)}$ only connects quark-antiquark condensates but no diquark condensates. Since, on the other hand, the coupling between quark-antiquark and diquark condensates was found to be important in the GL analysis of Refs. [22–24], the authors of Ref. [25] have introduced a second six-point interaction. In our notation, Eq. (4), this term can be written as

$$\mathcal{L}_{\chi d}^{(6)} = \frac{K'}{8}\sum_{i,j,k=1}^{3}\sum_{\pm}[(\bar{q}t_i l_k(1\pm\gamma_5)C\bar{q}^T) \times (q^T C(1\pm\gamma_5)t_j l_k q)(\bar{q}_i(1\pm\gamma_5)q_j)], \quad (6)$$

where in the last factor the indices i and j refer to the flavor components. $\mathcal{L}_{\chi d}^{(6)}$ has the same symmetries as Eq. (5), but the quark fields are ordered in such a way that in Hartree approximation the diquark and quark-antiquark condensates are connected. This reordering of the quark fields can be realized via a Fierz transformation[1] of the instanton vertex relating $\mathcal{L}_\chi^{(6)}$ to $\mathcal{L}_{\chi d}^{(6)}$. In this way, one can also relate the new coupling constant K' to K. However, following Ref. [25], we will treat K' as a free independent parameter.

B. Mean-field approximation and thermodynamic potential

We are working in mean-field approximation by introducing the scalar diquark condensates

$$s_i = \langle q^T C\gamma_5 t_i l_i q\rangle \quad (7)$$

[1]Useful references in this context are Refs. [39–41].

and the scalar antiquark-quark condensates

$$\phi_i = \langle \bar{q}_i q_i \rangle, \qquad i = 1, 2, 3. \tag{8}$$

In Hartree approximation the six-point interaction $\mathcal{L}^{(6)}_{\chi d}$ Eq. (6) then is simplified to

$$\mathcal{L}^{(6)}_{\chi d\,\mathrm{MF}} = \frac{K'}{4} \sum_{i=1}^{3} [-|s_i|^2 \bar{q}_i q_i - s_i^\star q^T C\gamma_5 t_i l_i q \phi_i + \bar{q}\gamma_5 t_i l_i C\bar{q}^T s_i \phi_i + 2|s_i|^2 \phi_i]. \tag{9}$$

One can identify the first term as a contribution to the effective quark masses, while the following two terms contribute to the anomalous self-energy of the propagator in the color superconducting phase. The last term does not depend on the fields and gives a constant contribution.

Adding the other terms from Eq. (1) and using Nambu-Gorkov bispinors $\Psi^T = 1/\sqrt{2}(q, C\bar{q}^T)$ the full mean-field Lagrangian can be written as

$$\mathcal{L}^{\mathrm{MF}} = \bar{\Psi} S^{-1} \Psi - \mathcal{V}, \tag{10}$$

with the inverse dressed propagator

$$S^{-1}(p) = \begin{pmatrix} \not{p} + \mu\gamma_0 - \hat{M} & \sum_{i=1}^{3} \Delta_i \gamma_5 t_i l_i \\ -\sum_{i=1}^{3} \Delta_i^\star \gamma_5 t_i l_i & \not{p} - \mu\gamma_0 - \hat{M} \end{pmatrix}. \tag{11}$$

Here $\hat{M}$ is the diagonal mass matrix of the constituent quark masses with the components

$$M_i = m_i - 4G\phi_i + K|\epsilon_{ijk}|\phi_j\phi_k + \frac{K'}{4}|s_i|^2. \tag{12}$$

The off-diagonal elements of Eq. (11) include

$$\Delta_i = -2\left(H - \frac{K'}{4}\phi_i\right)s_i. \tag{13}$$

Finally, $\mathcal{L}^{\mathrm{MF}}$ includes a field-independent term

$$\mathcal{V} = 2G\sum_{i=1}^{3}\phi_i^2 - 4K\phi_1\phi_2\phi_3 + \sum_{i=1}^{3}\left(H - \frac{K'}{2}\phi_i\right)|s_i|^2. \tag{14}$$

With these ingredients the thermodynamic potential in mean-field approximation becomes

$$\Omega(T, \mu) = -T\sum_n \int \frac{d^3p}{(2\pi)^3}\,\frac{1}{2}\,\mathrm{Tr}\ln\left(\frac{S^{-1}(i\omega_n, \vec{p})}{T}\right) + \mathcal{V}, \tag{15}$$

where the sum is over fermionic Matsubara frequencies. For equal diquark condensates $s_1 = s_2 = s_3 \equiv s$ and equal chiral condensates $\phi_1 = \phi_2 = \phi_3 \equiv \phi$, it agrees with the thermodynamic potential of Ref. [25], where only this limit was considered.

The self-consistent mean-field solutions are given by the stationary points of Ω with respect to the condensates, i.e., by the solutions of the gap equations

$$\frac{\partial\Omega}{\partial\phi_i} = \frac{\partial\Omega}{\partial s_i} = 0, \qquad i = 1, 2, 3. \tag{16}$$

The phase diagram is then constructed by taking the solution with the highest pressure (i.e., the lowest value of Ω) at each point in the μ-T plane.

C. Parameters

The model defined above contains eight parameters: the three bare quark masses (m_u, m_d, m_s), the two four-point coupling constants (G, H), the two six-point coupling constants (K, K'), and a regularization parameter. For the latter, we take a sharp three-momentum cutoff Λ.

To fix these parameters, we basically follow the procedure of Ref. [25]. Starting points are the parameters of Ref. [42],

$$\begin{aligned} &m_u = m_d = 5.5\ \mathrm{MeV}, \qquad m_s = 140.7\ \mathrm{MeV}, \\ &\Lambda = 602.3\ \mathrm{MeV}, \qquad G = 1.835/\Lambda^2, \\ &K = 12.36/\Lambda^5, \end{aligned} \tag{17}$$

which have been obtained by fitting meson masses and decay constants in vacuum. The value of the quark-quark coupling H, which cannot be determined from vacuum meson properties, is taken from Ref. [9],

$$H = 1.74/\Lambda^2. \tag{18}$$

Finally, as already mentioned, we treat the coupling constant K' as a free parameter. We will often take $K' = 4.2K$, because with this value a second endpoint was found in Ref. [25].

The authors of Ref. [25] have only studied the case of equal quark masses. To that end, they reduced the bare strange-quark mass to the value of the up and down quark masses and then readjusted the antiquark-quark coupling G, so that the dynamical up and down quark masses $M_u = M_d$ remain unchanged in vacuum (parameter set II of Ref. [25]):

$$m_s = m_u = m_d = 5.5\ \mathrm{MeV}, \qquad G = 1.918/\Lambda^2. \tag{19}$$

In this way, the vacuum values of the chiral condensates $\phi_u = \phi_d$ and of the pion mass and decay constant remain unchanged as well.

Since we are interested in the effect of the strange-quark mass on the phase structure, we generalize this procedure to the case of arbitrary values of m_s. Starting with equal quark masses, Eq. (19), we will increase the bare strange-quark mass up to the more realistic case, Eq. (17), always keeping the dynamical vacuum masses $M_u = M_d$ fixed by adjusting the coupling constant G.

III. RESULTS

In this section, we present our numerical results, which mainly consist of a series of phase diagrams with different six-point couplings K' and different choices for the

strange-quark mass. We begin with the case of equal bare quark masses in Sec. III A before introducing larger values of m_s in Sec. III B.

A. Equal bare masses

As a basis for our investigations, we consider equal quark masses $m_u = m_d = m_s = 5.5$ MeV and allow for only one common chiral condensate $\phi_1 = \phi_2 = \phi_3$ and one common diquark $s_1 = s_2 = s_3$. For $K' = 4.2K$, we then reproduce the phase diagram obtained in Ref. [25], as shown in Fig. 1. The normal phases, where all diquark condensates vanish, are denoted by "χSB" in regions with large chiral condensates and by "NQ" in regions with small chiral condensates. At low chemical potential and high temperature these two regions are connected by a crossover, while at higher chemical potential and lower temperature they are separated by a first-order phase boundary. Without diquark condensates the latter would continue down to the chemical-potential axis. However, when diquark condensates are included, the CFL phase is favored in the lower right part of the phase diagram, replacing the NQ phase in that regime. The first-order chiral phase transition then does no longer go down to zero temperature but ends inside the CFL phase,[2] while the latter is bordered to the χSB phase by a second-order phase boundary.

As discussed in Ref. [25], this particular phase structure is a consequence of the interaction term $\mathcal{L}^{(6)}_{\chi d}$. Without this term, i.e., for $K' = 0$, the χSB-CFL phase transition is first order and basically a continuation of the first-order χSB-NQ phase transition (see Fig. 4 below). In particular, the chiral condensate drops considerably at the phase boundary and is therefore small in the entire CFL phase. This is different for sufficiently large values of K', as in Fig. 1. In this case, the coupling between chiral and diquark condensates leads to the existence of strongly bound diquarks in the χSB phase, which eventually condense and then form a Bose-Einstein condensate (BEC) in the lower-μ part of the CFL phase (see also Ref. [43]). Hence, the χSB-CFL phase boundary is simply the condensation line of the diquarks, and therefore the transition is continuous. In particular, the chiral condensate is still large at the phase boundary and only decreases considerably at somewhat higher values of μ. In a small regime near the boundary to the NQ phase this happens discontinuously and is just the continuation of the first-order phase transition between the χSB and the NQ phase. At most temperatures, however, the decrease is continuous and closely related to a BEC-BCS crossover where the BEC-like CFL phase ("$\mathrm{CFL_{BEC}}$") gets converted into a BCS-like CFL phase

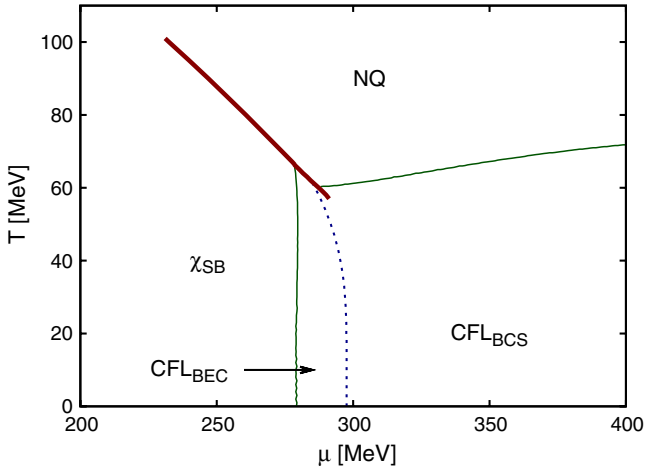

FIG. 1 (color online). The phase diagram in the μ-T plane for $K' = 4.2K$ and equal bare quark masses $m_u = m_d = m_s = 5.5$ MeV, only allowing for one common diquark condensate s and one common chiral condensate ϕ. Thick (red) solid lines denote first-order phase transitions, thin (green) solid lines second-order phase transitions. The dotted (blue) line indicates the BEC-BCS crossover line defined by $M(T, \mu) = \mu$, where $M \equiv M_u = M_d = M_s$.

("$\mathrm{CFL_{BCS}}$"). The corresponding crossover line is indicated in the figure as well. Following Ref. [25], we have defined it as the line where the in-medium constituent quark masses are equal to μ. Note that with this definition the crossover line does not exactly run into the endpoint of the first-order phase boundary.

Next, we allow the different diquark condensates s_i and the chiral condensates ϕ_i to vary independently for $i = 1, 2, 3$. This opens the possibility for the formation of a 2SC phase ($s_1 = s_2 = 0$, $s_3 \neq 0$). Still keeping the bare quark masses equal, we obtain the phase diagram shown in Fig. 2. Whereas, the normal-conducting phases NQ and χSB

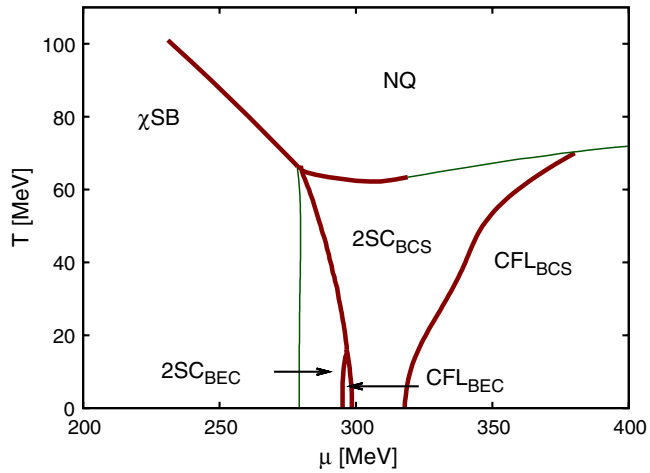

FIG. 2 (color online). The same as Fig. 1 but with independent diquark condensates s_1, s_2, s_3, and chiral condensates ϕ_1, ϕ_2, ϕ_3.

[2]In this article we use the term "chiral phase transition" whenever the transition is mainly characterized by a change of the chiral condensates ϕ_i. Note, however, that in the CFL phase chiral symmetry is always broken by the diquark condensates.

occupy approximately the same regions of the phase diagram as in Fig. 1, we find that a large part of the CFL phase is replaced by a 2SC phase. The first-order chiral phase transition, which in Fig. 1 ends inside the CFL phase, now separates a BEC-like 2SC phase with large chiral condensates ("$2SC_{BEC}$") and a BCS-like 2SC phase with small chiral condensates ("$2SC_{BCS}$"). However, unlike in Fig. 1, the BEC-like and the BCS-like phases are always separated by a first-order phase transition and never connected by a crossover.

Since s_1 and s_2 vanish in the 2SC phase, whereas they are equal to s_3 in the CFL phase, the two phases are necessarily separated by first-order phase boundaries. On the other hand, the phase transition from the CFL phase as well as from the neighboring region of the 2SC phase to the NQ phase is of second order.[3] As an interesting consequence, the first-order 2SC-CFL phase-transition line ends exactly on the second-order phase boundary to the NQ phase. Also note that the 2SC-NQ phase boundary, in the regime where it is second order, exactly agrees with the CFL-NQ phase boundary in Fig. 1. This is due to the fact that on the second-order phase boundary all diquark condensates vanish and therefore the 2SC phase and the CFL phase have the same free energy. For similar reasons, the second-order χSB-$2SC_{BEC}$ phase boundary agrees with the χSB-CFL_{BEC} phase boundary in Fig. 1. Again, this is not surprising because both boundaries are related to the Bose-Einstein condensation of diquarks, which are identical in the χSB phase and, hence, on the boundary.

At low temperatures ($T < 16$ MeV), we find a small area between the $2SC_{BEC}$ phase and the $2SC_{BCS}$ phase, where the CFL_{BEC} phase is slightly preferred. The origin of this "CFL island" will become more clear below.

In order to get a more complete picture, we now vary the coupling constant K' of the six-point interaction $\mathcal{L}^{(6)}_{\chi d}$. In Fig. 3, we show the phase diagram in the μ-K' plane for $T = 0$. One immediately recognizes that for all choices of K' there is always a first-order phase transition at some value of μ. For low values of K' only the χSB phase and the CFL phase are present. The first interesting development occurs when the interaction gets strong enough to have bound diquarks in the χSB phase, which then condense at some value of μ. As a consequence, a $2SC_{BEC}$ phase appears in the phase diagram. At a slightly higher value of K', the CFL phase splits into a BEC-like and a BCS-like region. These two regimes are separated by a first-order transition, which eventually turns into a crossover at higher values of K'. The corresponding endpoint marks the critical value of K', where in the phase diagram with equal condensates ($s_1 = s_2 = s_3$, $\phi_1 = \phi_2 = \phi_3$) the lower critical end point appears on the μ axis.

[3]For simplicity, we drop the subscripts "BCS" or "BEC" when the distinction between BCS-like or BEC-like phases is not relevant for the discussion.

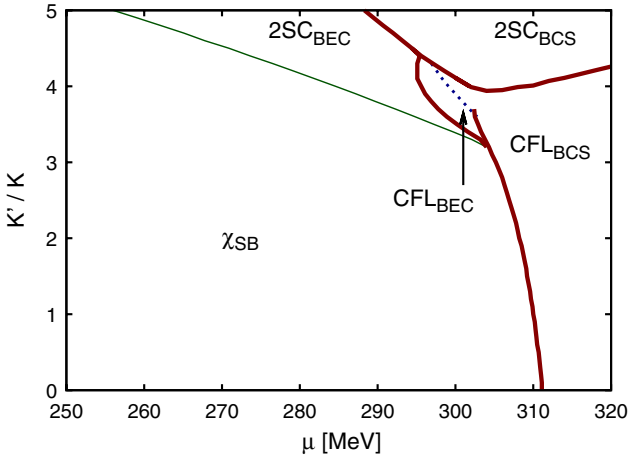

FIG. 3 (color online). The phase diagram in the μ-K' plane at $T = 0$ for equal quark masses $m_u = m_d = m_s = 5.5$ MeV. The meaning of the different line types is the same as in Fig. 1.

However, allowing for 2SC pairing, there still is a first-order transition between the $2SC_{BEC}$ and the CFL_{BEC} phase.

Cutting Fig. 3 at $K' = 4.2K$, we reproduce the $T = 0$ behavior of Fig. 2. From this perspective it becomes clear that the CFL island, which we have found there between the $2SC_{BEC}$ and the $2SC_{BCS}$ phase, corresponds to the upper end of the CFL_{BEC} regime and will disappear at a slightly higher value of K'.

In Fig. 4, we show a series of phase diagrams in the μ-T plane in order to illustrate how the phase structure evolves with K'. While the effect is almost negligible for small and moderate values of K', a major restructuring takes place at $K' \gtrsim 3K$: It starts with a $2SC_{BCS}$ phase, which appears near the triple point of the three original phases 4(b) and then grows towards lower temperatures and higher chemical potentials. Slightly below $K' = 3.5K$, Bose condensation of diquarks sets in, leading to a $2SC_{BEC}$ phase and shortly afterwards to a CFL_{BEC} phase 4(c). At the beginning, the latter is completely separated from the CFL_{BCS} phase by a first-order phase boundary, which turns into a crossover upon further increasing K'. As a result, we find at $K' = 3.744K$ a critical endpoint 4(d), which is of the same origin as the low-temperature critical endpoint in Fig. 1. Note, however, that the endpoint is now located in a region which is separated from the low-density regime by a first-order phase transition between 2SC and CFL phase. Moreover, the endpoint exists only in an extremely small interval of the coupling K'. While for $K' = 3.743K$ the CFL_{BEC}-CFL_{BCS} phase transition is still first order down to $T = 0$; already at $K' = 3.745K$ the entire phase boundary including the endpoint is covered by the 2SC phase. Eventually, the latter reaches the μ axis and the two CFL regimes become separated again 4(e). At even higher K', the first-order $2SC_{BEC}$-$2SC_{BCS}$ phase transition turns into a

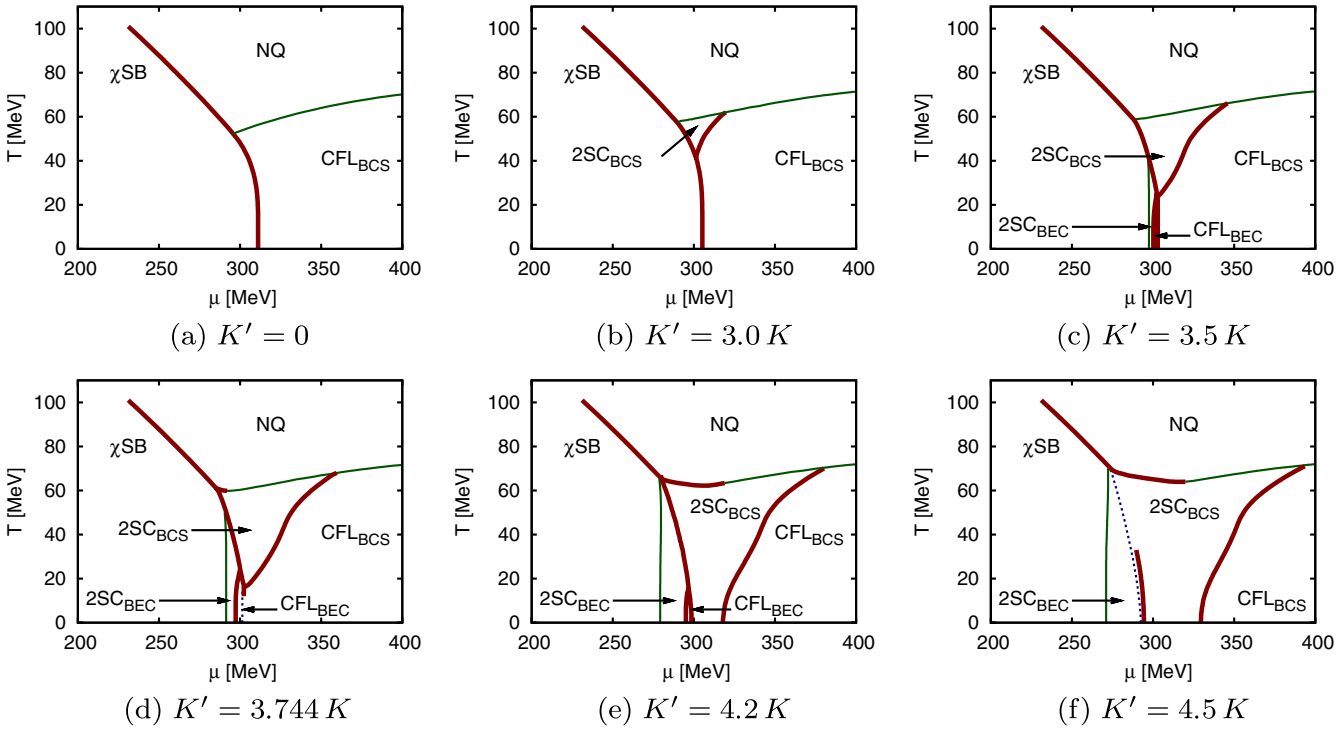

FIG. 4 (color online). The μ-T-phase diagram for different choices of K' and equal bare quark masses of ($m_u = m_d = m_s = 5.5$ MeV). The meaning of the different line types is the same as in Fig. 1. In the 2SC phase, the BEC-BCS crossover line (blue dotted line) is defined by the condition $M_{u,d}(T, \mu) = \mu$.

crossover, leading to another endpoint 4(f).[4] This endpoint is located at the upper temperature end of the first-order boundary, like the "conventional" endpoint of the χSB-NQ phase boundary, and it moves downwards with increasing K'. Finally, slightly above $K' = 5K$, it reaches the μ axis and only a crossover remains (not shown). On the other hand, as argued before, the 2SC-CFL phase transition is necessarily first order, and therefore there is always a discontinuous phase transition at low temperatures.

After getting this overview, we would like to understand how the 2SC phase can be preferred over the CFL phase in some regions of the phase diagram although we have chosen equal bare quark masses. It clearly means that the $SU(3)$-flavor symmetry is spontaneously broken, so there is in fact a continuous set of degenerate ground states, which are related to each other by flavor rotations. Bearing in mind that we will introduce larger strange-quark masses later on, we choose, without loss of generality, the standard 2SC pairing pattern, i.e., $s_3 \neq 0$, $s_1 = s_2 = 0$.

As obvious from Figs. 3 and 4, the emergence of the 2SC phase at equal bare quark masses is a consequence of the six-point interaction $\mathcal{L}^{(6)}_{\chi d}$. This term couples the chiral condensates to the diquark condensates and, thus, the constituent quark masses to the diquark gaps, see Eqs. (12) and (13). However, whereas in the CFL phase this happens symmetrically for all flavors, in the 2SC phase these equations conspire in a rather peculiar way: Since $s_3 \neq 0$ but $s_1 = s_2 = 0$, there is a contribution from the diquark condensates to M_s but not to M_u and M_d. Hence, even if we start with equal bare quark masses, in the 2SC phase the strange quarks will be heavier than the non-strange quarks. In turn, the larger value of M_s leads to an enhancement of Δ_3 via an increased modulus of the (negative) condensate ϕ_3 in Eq. (13).

This effect is illustrated in Fig. 5, where the diquark gap parameters and the constituent quark masses are shown as functions of the six-point coupling strength K' for the CFL and 2SC solutions at $T = 0$ and $\mu = 310$ MeV. One can clearly see that Δ_3 and M_s in the 2SC phase rise much faster with K' than the other quantities shown in the figure. In particular, the ratio between Δ_3 in the 2SC phase and the common gap parameter Δ in the CFL phase rises from about 1.25 at $K' = 0$ to 2.0 at $K' = 4$. It is therefore plausible that eventually the gain in free-energy is larger for 2SC pairing than for CFL pairing. In fact, if we had only diquark condensates and no dynamical quark masses, the pairing energy would be proportional to Δ_i^2 for each quasiparticle mode with pairing gap Δ_i. 2SC pairing would then be favored for $\Delta_3|_{\mathrm{2SC}} > \sqrt{3}\Delta|_{\mathrm{CFL}}$. Although in our

[4]As mentioned earlier, the BEC-BCS crossover line (blue dotted line), which we have defined as the line where the non-strange constituent quark masses are equal to μ, does not exactly run into the endpoint. In this sense, the first-order phase transition (related to a discontinuity in the condensates) does not exactly coincide with the BEC-BCS transition, although both are closely related to each other.

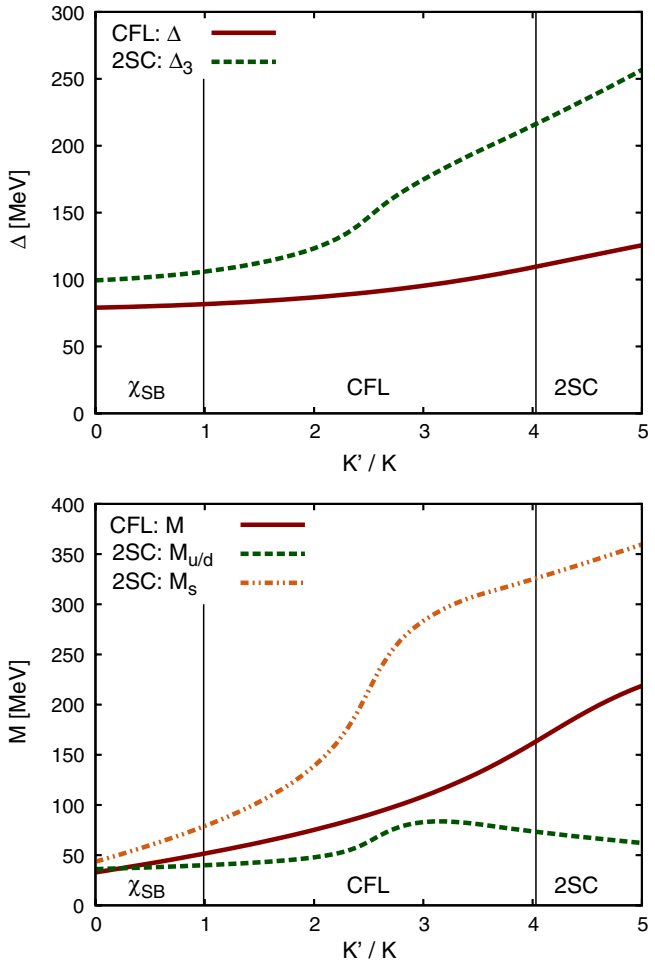

FIG. 5 (color online). The gap parameters Δ_i (upper panel) and the constituent quark masses M_i (lower panel) in the 2SC and CFL solutions as functions of K' for $m_u = m_d = m_s = 5.5$ MeV at $T = 0$ and $\mu = 310$ MeV. The vertical lines indicate the values of K', where the phase transitions from χSB to CFL or from CFL to 2SC take place (cf. Fig. 3).

case, the dynamical quark masses (and their coupling to the diquark condensates) are crucial and certainly cannot be neglected, this estimate can at least roughly explain the numerical results.

At first sight, the results found in this section seem to contradict the GL analysis of Refs. [22–24], where no 2SC-like solution was found for three equal flavors. However, although starting from a general GL potential, the authors have chosen a particular ansatz for the condensates, which does not allow for such solutions. By making a more general ansatz, one can show that our results are indeed consistent with the GL analysis. This is discussed in more detail in the Appendix.

B. Realistic strange-quark mass

We now introduce bare strange-quark masses that are larger than the masses of the up and down quarks. In particular, we are interested in $m_s = 140.7$ MeV, which is the value obtained in Ref. [42] by fitting vacuum meson properties. We begin, however, with a more systematic investigation of the mass effects by gradually increasing m_s from the equal-mass case $m_s = 5.5$ MeV to the "realistic" value $m_s = 140.7$ MeV. Thereby, we adjust the coupling G for each value of m_s as described in Sec. II C.

The phase diagram in the μ-m_s plane at $T = 0$ for $K' = 4.2K$ is shown in Fig. 6. As usual, we now define the CFL phase as a phase where all three diquark gaps Δ_i take nonvanishing values but do not need to be equal. With rising m_s, since pairs involving strange quarks become increasingly disfavored, the CFL phase gets more and more replaced by the 2SC phase, thus pushing the phase boundary to higher values of μ. As the spontaneous breaking of flavor $SU(3)$ through the mechanism described above is now stabilized by an explicit symmetry breaking, even a small enhancement of m_s has a rather large effect. For similar reasons, the small CFL area between the $2SC_{BEC}$ phase and the $2SC_{BCS}$ phase disappears already at $m_s \approx 7.5$ MeV. Above this point there is a first-order phase transition between the two 2SC phases, which ends at $m_s \approx 105$ MeV.

A larger value of m_s also leads to a larger value of the strange chiral condensate ϕ_3, which in turn leads to an enhancement of the effective four-point quark-quark coupling in the ud channel. The latter comes about from closing a strange-quark loop in the six-point interaction term $\mathcal{L}^{(6)}_{\chi d}$ and adding this contribution to the genuine four-point vertex from $\mathcal{L}^{(4)}_{d}$. As a consequence, the diquarks get bound more deeply, i.e., the diquark mass is reduced and, hence, their condensation, which determines the transition from the χSB phase to the $2SC_{BEC}$ phase, is shifted to lower quark chemical potential.

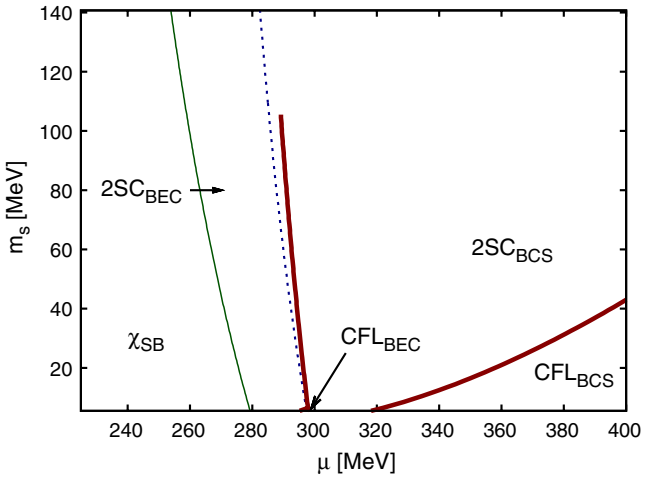

FIG. 6 (color online). The phase diagram in the μ-m_s plane at $T = 0$ for $K' = 4.2K$. The coupling G is adjusted with changing m_s as described in Sec. II C. Thick (red) lines denote first-order phase transitions, thin (green) lines second-order phase transitions. The blue dotted line indicates the BEC-BCS crossover line defined by $M_{u,d}(T, \mu) = \mu$.

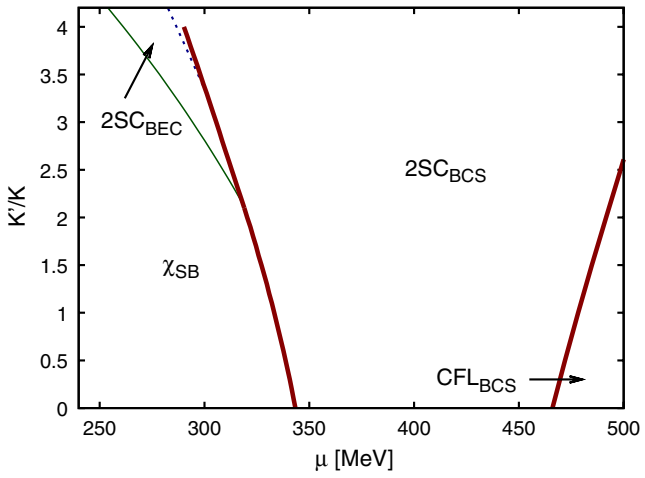

FIG. 7 (color online). The phase diagram in the μ-K' plane at $T = 0$ for $m_s = 140.7$ MeV. The meaning of the different line types is the same as in Fig. 6.

In the remaining part of this article, we fix the strange-quark mass at the realistic value, $m_s = 140.7$ MeV. In Fig. 7, we show the phase structure at $T = 0$ in dependence of the six-point coupling strength K'. With increasing K', the effective quark-quark coupling becomes stronger and the χSB-2SC phase transition moves to lower quark chemical potentials. Around $K' = 2.2K$, the $2SC_{BEC}$ phase forms at the low chemical potential side of the chiral phase-transition line. With larger K', this region becomes broader, and at $K' = 4.0K$ the first-order phase transition between the $2SC_{BEC}$ phase and the $2SC_{BCS}$ phase ends. Similar to the equal-mass case, we also find that an increase of K' is more favorable for the 2SC phase than for the CFL phase, so that the latter gets shifted to higher values of μ.

In Fig. 8, we finally show a series of phase diagrams in the μ-T plane for different values of K'. A general result is that none of them contains a critical endpoint at the low-temperature side of the first-order chiral phase transition. For $K' = 0$, we recover the standard phase diagram 8(a), which has been calculated, e.g., in Ref. [29] for the same parameters: At low temperature chiral symmetry is restored in a first-order phase transition between χSB and 2SC phase, which is continued by a first-order phase transition between χSB and NQ phase at higher temperatures and finally ends in a critical endpoint. Furthermore, there is a CFL phase at low temperature and high chemical potential. With increasing K', the 2SC pairing becomes strengthened so that the CFL phase is pushed to higher chemical potentials, while the first-order chiral phase transition gets successively "swallowed" by the expanding 2SC phase: As a first step the upwards-moving second-order 2SC-NQ phase boundary reaches the critical endpoint of the χSB-NQ phase boundary 8(b). Next, a $2SC_{BEC}$ phase emerges on the left-hand-side of the χSB-2SC phase boundary 8(c, d), and eventually the condensation line unites with the $2SC_{BCS}$-NQ phase boundary 8(e). At the same time, first-order chiral symmetry restoration line becomes disconnected and ends inside the

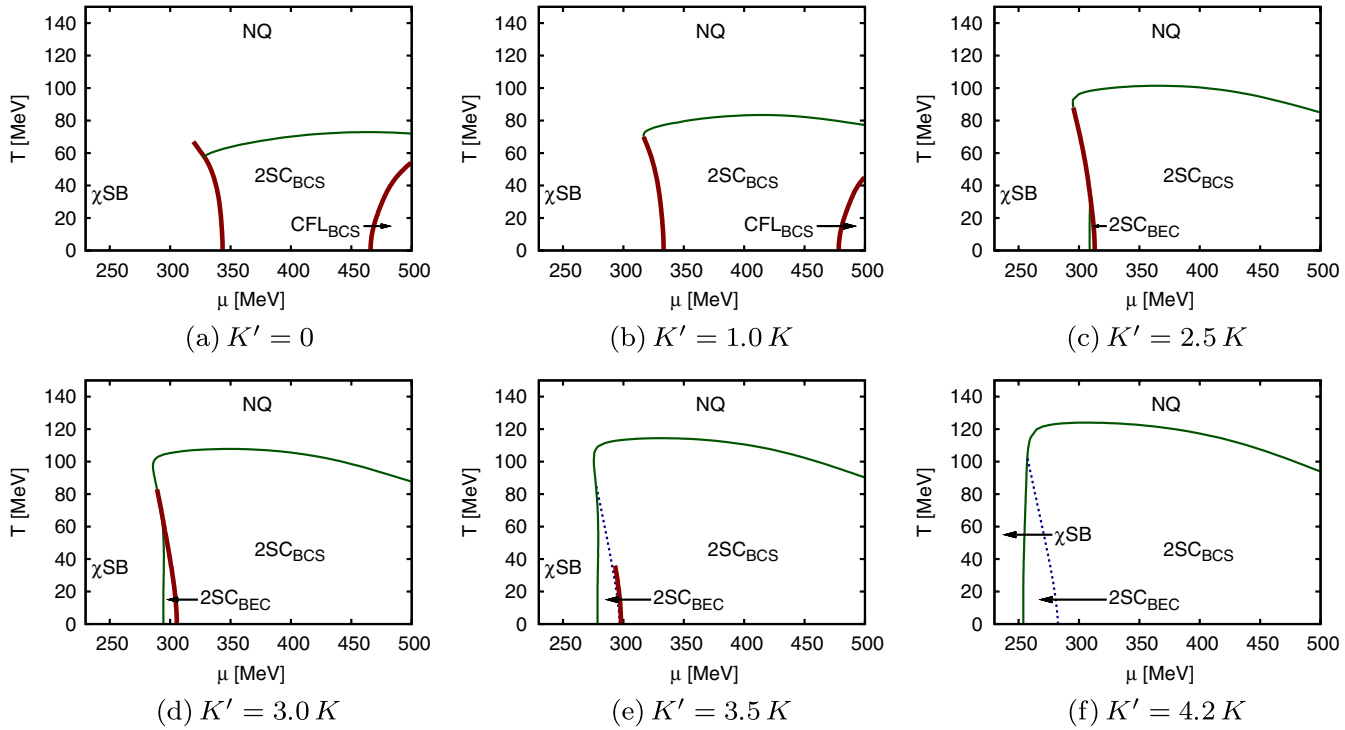

FIG. 8 (color online). The (μ-T)-phase diagram for different choices of K' and a bare strange-quark mass of $m_s = 140.7$ MeV. The meaning of the different line types is the same as in Fig. 6.

2SC phase. When K' is further increased, the endpoint moves downwards in temperature and finally disappears completely 8(f).

IV. CONCLUSIONS

We have investigated the phase structure of strongly interacting matter within a three-flavor NJL-type model with an extended six-point interaction that couples chiral and diquark condensates. This interaction term, which is usually neglected in NJL-model studies of the phase diagram, has been introduced in Ref. [25] and mimics effects of the axial anomaly. While this in principle leads to a more complete picture, the corresponding coupling constant K' is basically unknown and was therefore treated as a free parameter in our analysis.

Aim of the present study was to extend the investigations of Ref. [25] to realistic strange-quark masses. In this context, we have generalized the mean-field ansatz to allow for flavor-dependent chiral and diquark condensates. This opens the possibility for 2SC pairing, which was expected to become relevant at large strange-quark masses.

It turned out, however, that even for equal bare quark masses, the 2SC phase is present in the phase diagram if the coupling K' is sufficiently strong. This spontaneous breaking of the $SU(3)$ flavor symmetry occurs because the axial anomaly induces a mutual amplification of the strange chiral condensate and the nonstrange diquark condensate. As an important consequence, we have not found a continuous transition from the low-density chirally broken phase to the CFL phase at $T = 0$ for any value of K' between $K' = 0$ and $K' = 5K$. Related to this, the low-temperature critical end point which was found in Ref. [25] only survives in an extremely narrow K' interval and is otherwise covered by the 2SC phase.

As expected, the 2SC phase plays an even more important role at larger bare strange-quark masses, in particular, for the ''realistic value'', taken from a fit to vacuum observables. By varying K', we find several qualitatively different phase diagrams, where the first-order chiral phase transition ends outside, inside, or on the phase boundary of the 2SC phase, or where there is no first-order chiral phase transition at all. It should be noted, however, that most of these qualitative changes only occur at relatively large values of K', which may turn out to be unrealistic. But even for smaller couplings, the anomaly can be quantitatively important, as it stabilizes the 2SC pairing and shifts the CFL phase to higher chemical potentials.

The present study may be seen as a minimal extension of the analysis of Ref. [25] to include realistic strange-quark masses. There are, however, many other aspects which have not yet been taken into account. Perhaps most important is the consideration of inhomogeneous phases. For a two-flavor NJL model without color superconductivity, it has been shown that the entire first-order chiral phase-transition line is covered by an inhomogeneous region and therefore removed from the phase diagram [44–46]. It would be interesting to see how this result is modified when strange quarks and color superconducting phases are included, and how the results depend on the axial anomaly.

We have also neglected the possibility of kaon condensation in the CFL phase [47], which was found to be very important in an NJL model with realistic strange-quark masses [34,35]. In these references, on the other hand, the anomaly effects described by $\mathcal{L}^{(6)}_{\chi d}$ have not been taken into account. This term should lead to a higher kaon mass and therefore suppress its condensation. It would be interesting to study this in more detail.

Finally, we should recall that we have restricted ourselves to a single quark chemical potential. Similar investigations of anomaly effects should also be performed for electrically and color neutral matter.

ACKNOWLEDGMENTS

The work of H. B. was supported by the Helmholtz International Center for FAIR and by the Helmholtz Graduate School for Hadron and Ion Research. M. B. acknowledges partial support by EMMI.

APPENDIX: GINZBURG-LANDAU APPROACH

The most general expression for the GL free energy up to order four is given in the equations (7), (13) and (14) in Ref. [23] as the difference to the normal phase

$$\Omega(\Phi, d_L, d_R) = \Omega_\chi(\Phi) + \Omega_d(d_R, d_L) + \Omega_{\chi d}(\Phi, d_R, d_L) \tag{A1}$$

with

$$\begin{aligned}
\Omega_\chi &= \frac{a_0}{2}\,\mathrm{Tr}[\Phi^\dagger\Phi] + \frac{b_1}{4!}(\mathrm{Tr}[\Phi^\dagger\Phi])^2 + \frac{b_2}{4!}\,\mathrm{Tr}[(\Phi^\dagger\Phi)^2] - \frac{c_0}{2}(\det[\Phi] + \det[\Phi^\dagger]),\\
\Omega_d &= \alpha_0\,\mathrm{Tr}[d_L d_L^\dagger + d_R d_R^\dagger] + \beta_1((\mathrm{Tr}[d_L d_L^\dagger])^2 + (\mathrm{Tr}[d_R d_R^\dagger])^2) + \beta_2\,\mathrm{Tr}[(d_L d_L^\dagger)^2 + (d_R d_R^\dagger)^2] + \beta_3\,\mathrm{Tr}[(d_R d_L^\dagger)(d_L d_R^\dagger)]\\
&\quad + \beta_4\,\mathrm{Tr}[d_L d_L^\dagger]\mathrm{Tr}[d_R d_R^\dagger],\\
\Omega_{\chi d} &= \gamma_1\,\mathrm{Tr}[(d_R d_L^\dagger)\Phi + (d_L d_R^\dagger)\Phi^\dagger], + \lambda_1\,\mathrm{Tr}[(d_L d_L^\dagger)\Phi\Phi^\dagger + (d_R d_R^\dagger)\Phi^\dagger\Phi], + \lambda_2\,\mathrm{Tr}[d_L d_L^\dagger + d_R d_R^\dagger]\cdot\mathrm{Tr}[\Phi^\dagger\Phi]\\
&\quad + \lambda_3(\det[\Phi]\cdot\mathrm{Tr}[(d_L d_R^\dagger)\Phi^{-1}] + \mathrm{H.c.}).
\end{aligned} \tag{A2}$$

Here, Φ, d_L, and d_R are 3×3 matrices containing the chiral and the left- and right-handed diquark fields, respectively, (for details, see Ref. [23]). This ansatz has 13 unknown coefficients, which are in general T and μ dependent functions and cannot be determined within the GL analysis.

For the investigation of three massless flavors, the authors of Ref. [23] have therefore restricted themselves to an ansatz with equal condensates for all flavors, $\Phi = \mathrm{diag}(\sigma, \sigma, \sigma)$ and $d_L = -d_R = \mathrm{diag}(d, d, d)$. The free energy then takes the simplified form

$$\Omega_{3F}(\sigma, d) = \left(\frac{a}{2}\sigma^2 - \frac{c}{3}\sigma^3 + \frac{b}{4}\sigma^4\right) + \left(\frac{\alpha}{2}d^2 + \frac{\beta}{4}d^4\right) - \gamma d^2\sigma + \lambda d^2\sigma^2 \tag{A3}$$

with only seven independent coefficients,[5] which are related to the original GL coefficients in Eq. (A2) by

$$\begin{aligned} &a = 3a_0, \qquad c = 3c_0, \qquad b = \frac{1}{2}(3b_1 + b_2), \\ &\alpha = 12\alpha_0, \qquad \beta = 12(6\beta_1 + 2\beta_2 + \beta_3 + 3\beta_4), \\ &\gamma = 6\gamma_1, \qquad \lambda = 6(\lambda_1 + 3\lambda_2 - \lambda_3). \end{aligned} \tag{A4}$$

Yet, the full exploration of the remaining seven-dimensional parameter space would still be almost impossible. However, by making additional, physically motivated, assumptions (e.g., positivity of c, β, γ, and λ) interesting nontrivial results have been extracted in Refs. [22–24].

Similarly, two-flavor systems have been investigated in Ref. [23] choosing $\Phi = \mathrm{diag}(\sigma, \sigma, 0)$ and $d_L = -d_R = \mathrm{diag}(0, 0, d)$, i.e., by completely neglecting all condensates which involve strange quarks. The resulting free energy is given by

$$\Omega_{2F}(\sigma, d) = \left(\frac{a'}{2}\sigma^2 + \frac{b'}{4}\sigma^4\right) + \left(\frac{\alpha'}{2}d^2 + \frac{\beta'}{4}d^4\right) + \lambda' d^2\sigma^2, \tag{A5}$$

with five independent coefficients, which are different from those in Eq. (A3). In this context, it is important to note that by neglecting the strange condensates completely, it was assumed that the strange quarks are infinitely heavy and therefore decouple from the nonstrange sector. In particular, a direct comparison of Ω_{2F} with Ω_{3F} in order to study the competition between 2SC and CFL pairing was not intended and is not possible.

In contrast, in our NJL-model anlysis, we have studied a 2SC phase in a three-flavor environment with a large strange-quark chiral condensate. The corresponding GL ansatz is $\Phi = \mathrm{diag}(\sigma, \sigma, \sigma_s)$ and $d_L = -d_R = \mathrm{diag}(0, 0, d)$, yielding

$$\Omega_{2\mathrm{SC}}(\sigma, \sigma_s, d) = \left(\frac{a}{2}\frac{2\sigma^2 + \sigma_s^2}{3} - \frac{c}{3}\sigma^2\sigma_s + \frac{b_1'}{4}\sigma^4 + \frac{b_2'}{4}\sigma_s^4 + \frac{b_1' - 2b_2'}{2}\sigma^2\sigma_s^2\right) + \left(\frac{\alpha}{6}d^2 + \frac{\beta'}{4}d^4\right) - \frac{\gamma}{3}d^2\sigma_s + \lambda_1' d^2\sigma^2 + \lambda_2' d^2\sigma_s^2, \tag{A6}$$

where the coefficients a, c, α, and γ are the same as in Eq. (A4), and

$$\begin{aligned} b_1' &= \frac{1}{3}(2b_1 + b_2), \\ b_2' &= \frac{1}{6}(b_1 + b_2), \\ \beta' &= 4(2\beta_1 + 2\beta_2 + \beta_3 + \beta_4), \\ \lambda_1' &= 2(2\lambda_2 - \lambda_3), \\ \lambda_2' &= 2(\lambda_1 + \lambda_2). \end{aligned} \tag{A7}$$

Hence, instead of five GL coefficients as in Eq. (A5), $\Omega_{2\mathrm{SC}}$ depends on nine independent coefficients. In particular, unlike Ω_{2F}, it contains the anomaly induced c and γ terms, which are related to the six-point interactions Eqs. (5) and (6) in the NJL-Lagrangian.

Obviously, the extra terms in Eq. (A6) are due to the strange chiral condensate σ_s, which is not present in Ω_{2F}. We can thus recover Eq. (A5) by setting σ_s equal to zero. In fact, a more appropriate way to describe the decoupling of the strange quarks with large masses is to treat σ_s as a nonvanishing constant. The γ term, among others, then leads to a renormalization of the d^2-coefficient α, while, e.g., the b_1' term leads to a shift of the vacuum energy. This underlines again that a direct comparison of the free energies obtained with Ω_{2F} and Ω_{3F} would be meaningless.

On the other hand, keeping σ_s as a dynamical variable, a comparison of Ω_{3F} with $\Omega_{2\mathrm{SC}}$ is possible.[6] To that end, we should replace the coefficient b in Eq. (A3) by the combination $3(b_1' - b_2')$ and the coefficient λ by $3(\lambda_1' + \lambda_2')$. Moreover, we have to take into account that the coefficients β and β' are linear independent [see Eqs. (A4) and (A7)]. This can be accounted for by writing $\beta = 3(3\beta_1' + \beta_2')$ and $\beta' = \beta_1' + \beta_2'$ with $\beta_1' = 4(2\beta_1 + \beta_4)$ and $\beta_2' = 4(2\beta_2 + \beta_3)$. Thus, in order to compare the free energies of the 2SC and CFL solutions, we have to deal with ten independent parameters[7] $(a, c, b_1', b_2', \alpha, \beta_1', \beta_2', \gamma, \lambda_1', \lambda_2')$, plus possible six-order terms which might be needed for stability reasons. An exhaustive GL analysis is therefore practically impossible.

[5] In addition, a term of order σ^6 must be introduced by hand in order to stabilize the system if $b < 0$. For simplicity, we neglect such terms in the present qualitative discussion.

[6] Here, we tacitly assume that the GL analysis is meaningful in both phases, i.e., that all condensates are small. Clearly, this does not need to be the case.

[7] A straightforward way to obtain a unified description of both CFL and 2SC phase is to make the ansatz $\Phi = \mathrm{diag}(\sigma, \sigma, \sigma_s)$ and $d_L = -d_R = \mathrm{diag}(d', d', d)$. In this case, there are 11 independent coefficients. Our approach is more restrictive and therefore has one parameter less.

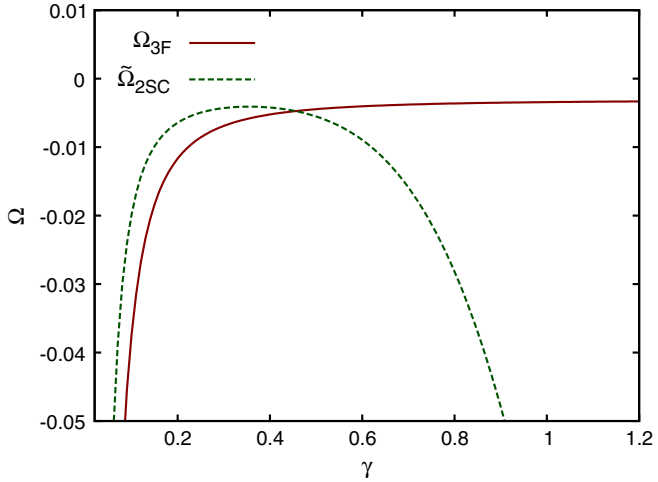

FIG. 9 (color online). The Ginzburg-Landau free energies of CFL solutions (solid) and 2SC solutions (dashed) as functions of γ at the endpoint found in Ref. [22–24] for the example described in the text.

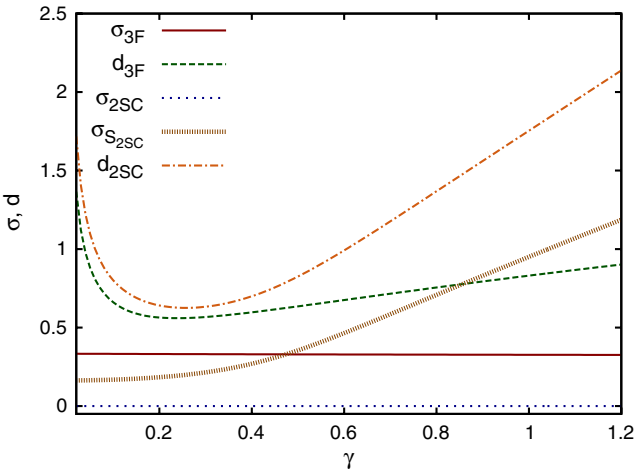

FIG. 10 (color online). The condensates which minimize the GL free energies in the examples given in Fig. 9.

However, since we only want to show that 2SC-like solutions can indeed be favored in some cases, it is sufficient to demonstrate this by an example. In order to proceed, we therefore make a few simplifying assumptions: (i) We neglect all λ terms, i.e, $\lambda_1 = \lambda_2 = \lambda = 0$. This was also done in Ref. [23] in the three-flavor case. (ii) In the NJL model without the anomaly terms and without diquark coupling, i.e., taking into account only the interaction term $\mathcal{L}_\chi^{(4)}$, the different flavors do not mix. Hence, their contributions to the thermodynamic potential are additive. To reproduce this feature, we choose $b_1' = 2b/3$, $b_2' = b/3$. (iii) In the diquark sector, we choose $\beta' = \beta/(3 \cdot 2^{2/3})$. In the absence of chiral condensates (or for $\gamma = 0$), this leads to the relation $d_{2SC} = 2^{1/3} d_{3F}$, in agreement with weak-coupling QCD [8]. As can be seen in Fig. 5, this relation is also approximately fulfilled in the NJL model at $K' = 0$. (iv) We restrict the possible 2SC solutions to BCS-like solutions, i.e., we set $\sigma = 0$ in Eq. (A6).

For the 2SC phase, we then obtain the simplified GL potential

$$\tilde{\Omega}_{2SC}(\sigma_s, d) = \left(\frac{a}{6}\sigma_s^2 + \frac{b}{12}\sigma_s^4\right) + \left(\frac{\alpha}{6}d^2 + \frac{\beta}{12 \cdot 2^{2/3}}d^4\right) - \frac{\gamma}{3}d^2\sigma_s, \tag{A8}$$

while the CFL phase is described by Eq. (A3) with $\lambda = 0$. Thereby both potentials depend on the same coefficients so that the resulting free energies can be compared with each other. In order to further reduce the number of parameters, we perform this comparison at the location of the low-temperature critical end point found in Ref. [22–24],

$$a = \frac{c^2}{3b} + \frac{2\gamma^2}{\beta}, \qquad \alpha = -\frac{\beta c^2}{27\gamma b^2}. \tag{A9}$$

This eliminates a and α from the equations, so that we are left with four parameters b, c, β, and γ.

Finally, we introduce an arbitrary scaling factor Λ of dimension energy and measure all dimensionful quantities in units of the corresponding power of Λ. We then simply choose $b = c = \beta = 1$ in these units and study the different free-energy solutions at the point given by Eq. (A9) for varying values of γ. This analysis has been done numerically.

In Fig. 9, we show the results for $\tilde{\Omega}_{2SC}$ and Ω_{3F} for our example. We see that the CFL solution is favored at low values of γ, whereas the 2SC solution becomes favored at larger values of γ. This phase transition is in qualitative agreement with our findings in the NJL model when K' is increased, cf. Fig. 3.

The values of the condensates associated with in minima of the free energy are shown in Fig. 10. Their behavior with rising γ is qualitatively similar to the effect of an increased K' in the NJL calculations, cf. Fig. 5. In both cases, when increasing the coupling (γ or K') the diquark and the strange-quark chiral condensate in the 2SC phase are rising much faster than the condensates in the CFL phase.

The NJL-model results are thus completely consistent with a GL analysis if the latter is performed with a sufficiently general ansatz for the condensates.

[1] P. Braun-Munzinger and J. Stachel, Nature (London) **448**, 302 (2007).
[2] M. Cheng *et al.*, Phys. Rev. D **81**, 054510 (2010).
[3] Y. Aoki, S. Borsanyi, S. Durr, Z. Fodor, S. D. Katz, S. Krieg, and K. K. Szabo, J. High Energy Phys. 06 (2009) 088.
[4] Y. Aoki, G. Endrodi, Z. Fodor, S. D. Katz, and K. K. Szabo, Nature (London) **443**, 675 (2006).
[5] K. Rajagopal and F. Wilczek, arXiv:hep-ph/0011333.
[6] M. G. Alford, Annu. Rev. Nucl. Part. Sci. **51**, 131 (2001).
[7] T. Schäfer, arXiv:hep-ph/0304281.
[8] D. H. Rischke, Prog. Part. Nucl. Phys. **52**, 197 (2004).
[9] M. Buballa, Phys. Rep. **407**, 205 (2005).
[10] I. A. Shovkovy, Found. Phys. **35**, 1309 (2005).
[11] M. G. Alford, A. Schmitt, K. Rajagopal, and T. Schäfer, Rev. Mod. Phys. **80**, 1455 (2008).
[12] D. T. Son, Phys. Rev. D **59**, 094019 (1999).
[13] T. Schäfer and F. Wilczek, Phys. Rev. D **60**, 114033 (1999).
[14] I. A. Shovkovy and L. C. R. Wijewardhana, Phys. Lett. B **470**, 189 (1999).
[15] T. Schäfer, Nucl. Phys. **B575**, 269 (2000).
[16] M. Asakawa and K. Yazaki, Nucl. Phys. **A504**, 668 (1989).
[17] J. Berges and K. Rajagopal, Nucl. Phys. **B538**, 215 (1999).
[18] M. A. Stephanov, K. Rajagopal, and E. V. Shuryak, Phys. Rev. Lett. **81**, 4816 (1998).
[19] M. Kitazawa, T. Koide, T. Kunihiro, and Y. Nemoto, Prog. Theor. Phys. **108**, 929 (2002).
[20] Z. Zhang, K. Fukushima, and T. Kunihiro, Phys. Rev. D **79**, 014004 (2009).
[21] Z. Zhang and T. Kunihiro, Phys. Rev. D **80**, 014015 (2009).
[22] T. Hatsuda, M. Tachibana, N. Yamamoto, and G. Baym, Phys. Rev. Lett. **97**, 122001 (2006).
[23] N. Yamamoto, M. Tachibana, T. Hatsuda, and G. Baym, Phys. Rev. D **76**, 074001 (2007).
[24] G. Baym, T. Hatsuda, M. Tachibana, and N. Yamamoto, J. Phys. G **35**, 104021 (2008).
[25] H. Abuki, G. Baym, T. Hatsuda, and N. Yamamoto, Phys. Rev. D **81**, 125010 (2010).
[26] M. G. Alford, K. Rajagopal, and F. Wilczek, Nucl. Phys. **B537**, 443 (1999).
[27] M. G. Alford, J. Berges, and K. Rajagopal, Nucl. Phys. **B558**, 219 (1999).
[28] M. Buballa and M. Oertel, Nucl. Phys. **A703**, 770 (2002).
[29] M. Oertel and M. Buballa, arXiv:hep-ph/0202098.
[30] R. Rapp, T. Schäfer, E. V. Shuryak, and M. Velkovsky, Phys. Rev. Lett. **81**, 53 (1998).
[31] M. G. Alford, K. Rajagopal, and F. Wilczek, Phys. Lett. B **422**, 247 (1998).
[32] S. B. Rüster, V. Werth, M. Buballa, I. A. Shovkovy, and D. H. Rischke, Phys. Rev. D **72**, 034004 (2005).
[33] H. Abuki and T. Kunihiro, Nucl. Phys. **A768**, 118 (2006).
[34] H. J. Warringa, arXiv:hep-ph/0606063.
[35] H. Basler and M. Buballa, Phys. Rev. D **81**, 054033 (2010).
[36] D. Blaschke, S. Fredriksson, H. Grigorian, A. M. Oztas, and F. Sandin, Phys. Rev. D **72**, 065020 (2005).
[37] M. Kobayashi and T. Maskawa, Prog. Theor. Phys. **44**, 1422 (1970).
[38] G. 't Hooft, Phys. Rev. D **14**, 3432 (1976); **18**, 2199(E) (1978); Phys. Rep. **142**, 357 (1986).
[39] V. Dmitrasinovic, J. Math. Phys. (N.Y.) **42**, 991 (2001); **45**, 2988(E) (2004).
[40] J. F. Nieves and P. B. Pal, Am. J. Phys. **72**, 1100 (2004).
[41] A. W. Steiner, Phys. Rev. D **72**, 054024 (2005).
[42] P. Rehberg, S. P. Klevansky, and J. Hufner, Phys. Rev. C **53**, 410 (1996).
[43] M. Kitazawa, D. H.Rischke, and I. A. Shovkovy, Phys. Lett. B **663**, 228 (2008).
[44] D. Nickel, Phys. Rev. Lett. **103**, 072301 (2009).
[45] D. Nickel, Phys. Rev. D **80**, 074025 (2009).
[46] S. Carignano, D. Nickel, and M. Buballa, Phys. Rev. D **82**, 054009 (2010).
[47] T. Schäfer, Phys. Rev. Lett. **85**, 5531 (2000).